Journal of Magnetic Resonance 197 (2009) 229–236

Contents lists available at ScienceDirect

Journal of Magnetic Resonance

journal homepage: www.elsevier.com/locate/jmr

Separation of isotropic chemical and second-order quadrupolar shifts by multiple-quantum double rotation NMR

Ivan Hung [a,1], Alan Wong [a], Andy P. Howes [a], Tiit Anupõld [b], Ago Samoson [b], Mark E. Smith [a], Diane Holland [a], Steven P. Brown [a], Ray Dupree [a,*]

[a] Physics Department, University of Warwick, Coventry, CV4 7AL, UK
[b] National Institute for Chemical Physics and Biophysics, Akadeemia Tee 23, Tallinn, Estonia

ARTICLE INFO

Article history:
Received 21 October 2008
Revised 6 January 2009
Available online 13 January 2009

Keywords:
Solid-state NMR
Double rotation
Multiple-quantum
Spectral shearing
Quadrupolar interaction
Chemical shift

ABSTRACT

Using a two-dimensional multiple-quantum (MQ) double rotation (DOR) experiment the contributions of the chemical shift and quadrupolar interaction to isotropic resonance shifts can be completely separated. Spectra were acquired using a three-pulse triple-quantum z-filtered pulse sequence and subsequently sheared along both the ν_1 and ν_2 dimensions. The application of this method is demonstrated for both crystalline ($RbNO_3$) and amorphous samples (vitreous B_2O_3). The existence of the two rubidium isotopes (^{85}Rb and ^{87}Rb) allows comparison of results for two nuclei with different spins ($I = 3/2$ and 5/2), as well as different dipole and quadrupole moments in a single chemical compound. Being only limited by homogeneous line broadening and sample crystallinity, linewidths of approximately 0.1 and 0.2 ppm can be measured for ^{87}Rb in the quadrupolar and chemical shift dimensions, enabling highly accurate determination of the isotropic chemical shift and the quadrupolar product, P_Q. For vitreous B_2O_3, the use of MQDOR allows the chemical shift and electric field gradient distributions to be directly determined—information that is difficult to obtain otherwise due to the presence of second-order quadrupolar broadening.

1. Introduction

In recent decades, solid-state NMR of quadrupolar nuclei has developed into an important technique for the characterization of structure and dynamics in condensed matter at an atomic scale. Quadrupolar nuclei (i.e., nuclei with magnetic spin $I > 1/2$) constitute ~75% of NMR-active nuclei in the Periodic Table and possess electric quadrupole moments which interact with any electric field gradient (EFG) present. This quadrupolar interaction produces broadening which often severely worsens the resolution of resonances. Various techniques have been devised in order to regain high-resolution/isotropic NMR spectra for half-integer quadrupolar nuclei ($I = 3/2$, 5/2, 7/2 and 9/2), namely, double rotation (DOR) [1,2], dynamic angle spinning (DAS) [1,3], multiple-quantum magic angle spinning (MQMAS) [4–6] and satellite transition (ST) MAS [7,8]. The former two techniques require dedicated equipment, whereas the latter two can be achieved using standard (commercial) solid-state NMR equipment. Therefore, since their inception MQMAS and STMAS have seen much greater popularity amongst researchers aiming to obtain isotropic NMR spectra of quadrupolar nuclei.

DOR is a technique capable of providing isotropic 1D spectra of quadrupolar nuclei in real time. Rather than relying on sophisticated pulse programming, DOR relies on mechanical sophistication in that the polycrystalline sample is spun simultaneously about two axes subtending the angles 54.74° and 30.56°. This process satisfies the conditions necessary to time-average both first- and second-order perturbations to the Zeeman interaction which have spatial dependences described by the second- and fourth-order Legendre polynomials, $P_2(\cos\beta)$ and $P_4(\cos\beta)$, respectively [1,2]. A number of studies have been reported utilizing DOR NMR for the differentiation of sodium, boron, aluminium and oxygen sites in minerals [9–11], materials [12–16] and molecular sieves, including, zeolites [17–20], sodalites [21–23] and aluminophosphates [24–28]. Recently, focus has turned to exploiting DOR for the study of oxygen sites in organic solids [29–35].

There has recently been renewed interest in the application of DOR NMR, not only for the resolution of quadrupolar sites, but also for the potential of obtaining additional structural information via the quantitative determination of anisotropic interactions. For example, the dipolar coupling and chemical shift anisotropy and their relative orientations can be determined from an analysis of DOR sideband patterns [34]. Two-dimensional MQDOR spectra

* Corresponding author. Fax: +44 (0)24 7652 3412.
E-mail address: R.Dupree@warwick.ac.uk (R. Dupree).
[1] Present address: CIMAR, National High Magnetic Field Laboratory, Tallahassee, FL 32310, USA.

1090-7807/$ - see front matter © 2009 Elsevier Inc. All rights reserved.
doi:10.1016/j.jmr.2009.01.005

have previously been presented [36–39]. Such a MQDOR spectrum can be transformed via shear and scaling transformations to give a two-dimensional representation in which the F_1 and F_2 frequencies correspond to the isotropic second-order quadrupolar shift and chemical shift, respectively [36–38]. In this paper, the protocol for such a transformation (for arbitrary spin quantum number and multiple-quantum coherence order) is presented together with the underlying theory. A complementary technique for separating chemical shift and quadrupolar *anisotropies* whilst spinning at 70.12° (named COASTER) has recently been reported [40]. MQDOR spectra are presented for crystalline $RbNO_3$ and vitreous B_2O_3. $RbNO_3$ is an ideal sample for examination of the MQDOR method as it provides two isotopes (^{85}Rb and ^{87}Rb) with different spin quantum numbers, Larmor frequencies and quadrupole moments. For v-B_2O_3, the effect of disorder on the isotropic chemical and quadrupolar shifts can be directly determined from the observed spectrum.

2. Theory

The theory underlying the DOR [34,41–43] and MQMAS [4–6] techniques, and the behavior of quadrupolar nuclei [44,45] has been examined thoroughly in the literature. Hence, only a brief summary of the necessary equations is presented herein with particular focus on the analysis and manipulation of the resulting spectra.

In a nuclear Zeeman system perturbed to second-order by the quadrupolar interaction, the difference in energy levels associated with symmetric transitions ($|m = p/2\rangle \leftrightarrow |\bar{m} = \bar{p}/2\rangle$), where p is the coherence order, for a single crystallite is given by

$$\Delta E^{Q(2)}_{S,p/2\leftrightarrow\bar{p}/2} = C_0(S,p)\nu_0^Q + C_2(S,p)\nu_2^Q - C_4(S,p)\nu_4^Q, \tag{1}$$

where the zeroeth-, second- and fourth-rank coefficients that depend on the spin angular momentum quantum numbers, S and $p = 2m$, are defined as follows:

$$C_0(S,p) = p\left[S(S+1) - \frac{3}{4}p^2\right], \tag{2}$$

$$C_2(S,p) = p[8S(S+1) - 3p^2 - 3], \tag{3}$$

$$C_4(S,p) = p\left[18S(S+1) - \frac{17}{2}p^2 - 5\right] \tag{4}$$

while the zeroeth-, second- and fourth-rank frequencies:

$$\nu_0^Q = \frac{3}{10}\frac{C_Q^2}{\nu_L[2S(2S-1)]^2}\Gamma_0, \tag{5}$$

$$\nu_2^Q = \frac{3}{28}\frac{C_Q^2}{\nu_L[2S(2S-1)]^2}\Gamma_2, \tag{6}$$

$$\nu_4^Q = \frac{9}{140}\frac{C_Q^2}{\nu_L[2S(2S-1)]^2}\Gamma_4, \tag{7}$$

depend on the orientation of the crystallite according to:

$$\Gamma_0(\eta_Q) = 1 + \frac{1}{3}\eta_Q^2, \tag{8}$$

$$\Gamma_2(\Omega_{PL},\eta_Q) = \left(1 - \frac{1}{3}\eta_Q^2\right)D^2_{00}(\Omega_{PL}) - \sqrt{\frac{2}{3}}\eta_Q\left[D^2_{20}(\Omega_{PL}) + D^2_{\bar{2}0}(\Omega_{PL})\right], \tag{9}$$

$$\Gamma_4(\Omega_{PL},\eta_Q) = \left(1 + \frac{1}{18}\eta_Q^2\right)D^4_{00}(\Omega_{PL}) + \frac{\sqrt{10}}{6}\eta_Q\left[D^4_{20}(\Omega_{PL}) + D^4_{\bar{2}0}(\Omega_{PL})\right], + \frac{\sqrt{70}}{36}\eta_Q^2[D^4_{40}(\Omega_{PL}) + D^4_{\bar{4}0}(\Omega_{PL})] \tag{10}$$

where the quadrupole coupling constant

$$C_Q = \frac{eQV_{33}}{h} \tag{11}$$

and asymmetry parameter

$$\eta_Q = \frac{V_{11} - V_{22}}{V_{33}} \tag{12}$$

correspond to the magnitude and degree of axial symmetry of the quadrupolar interaction, respectively. These two parameters are often combined, resulting in the composite quadrupole interaction constant (or quadrupolar interaction product)

$$P_Q = \sqrt{C_Q^2\Gamma_0} = C_Q\sqrt{1 + \eta_Q^2/3}. \tag{13}$$

$|V_{33}| \geqslant |V_{22}| \geqslant |V_{11}|$ and $\{V_{nn} \mid n = 1,2,3\}$ are the principal/diagonal components of the EFG tensor in its own principal axis system (PAS), and ν_L is the Larmor frequency in Hertz (Hz). The $D^j_{n'n}(\Omega_{PL})$ are j-rank Wigner rotation matrices [46] which depend on the angles $\Omega_{PL} = (\alpha_{PL}, \beta_{PL}, \gamma_{PL})$ relating the PAS (P) and laboratory (L) coordinate systems. For the case of magic angle spinning (MAS), $D^j_{n'n}(\Omega_{PL})$ can be expanded as follows

$$D^j_{n'n}(\Omega_{PL}) = \sum_{p=-j}^{j} D^j_{n'p}(\Omega_{PR})D^j_{pn}(\Omega_{RL}), \tag{14}$$

which performs a PAS (P) → rotor (R) → laboratory (L) transformation, whereas for double rotation (DOR),

$$D^j_{n'n}(\Omega_{PL}) = \sum_{q=-j}^{j}\sum_{p=-j}^{j} D^j_{n'p}(\Omega_{PI})D^j_{pq}(\Omega_{IO})D^j_{qn}(\Omega_{OL}) \tag{15}$$

which performs a PAS (P) → inner rotor (I) → outer rotor (O) → laboratory (L) frame transformation.

Application of DOR removes the two anisotropic terms in Eq. (1). Therefore, for a DOR experiment, with the additional inclusion of an isotropic chemical shift term, Eq. (1) can be expressed as

$$\Delta E^{CS,Q(2)}_{S,p/2\leftrightarrow\bar{p}/2} = -p\nu_0^{CS} + C_0(S,p)\nu_0^Q, \tag{16}$$

which corresponds to the position (in Hz) of resonance peaks in DOR spectra. The two terms in Eq. (16) are referred to as the isotropic chemical shift (ν_0^{CS}) and quadrupolar(-induced) shift (ν_0^Q) [45] for $p = -1$. These isotropic shifts will be denoted as δ_{CS} and δ_{QS} when given in units of parts per million (ppm), i.e.,

$$\delta_{CS} = \frac{\nu_0^{CS}}{\nu_L} \times 10^6 \tag{17}$$

and

$$\delta_{QS} = C_0(S,-1)\frac{\nu_0^Q}{\nu_L} \times 10^6. \tag{18}$$

Consider a two-dimensional multiple-quantum DOR experiment [36,37] that correlates coherence of order p' and p'' during t_1 and t_2, respectively. The resulting time-domain signal (neglecting relaxation effects) has the form

$$s(t_1,t_2) = \exp\left(i2\pi\cdot\Delta E^{CS,Q(2)}_{S,p'/2\leftrightarrow\bar{p}'/2}t_1\right)\exp\left(i2\pi\cdot\Delta E^{CS,Q(2)}_{S,p''/2\leftrightarrow\bar{p}''/2}t_2\right). \tag{19}$$

Using Eq. (16), (19) can be expanded as

$$s(t_1,t_2) = \exp\{-i2\pi\nu_0^{CS}[p't_1 + p''t_2]\}\exp\{i2\pi\nu_0^Q[C_0(S,p')t_1 + C_0(S,p'')t_2]\}. \tag{20}$$

In practice and by convention, the $p'' = -1$ transition is always observed during t_2, thence Eq. (20) becomes

$$s(t_1,t_2) = \exp\{-i2\pi\nu_0^{CS}[p't_1 - t_2]\}\exp\{i2\pi\nu_0^Q[C_0(S,p')t_1 + C_0(S,-1)t_2]\}, \tag{21}$$

and the gradients of ν_0^{CS} and ν_0^{Q} in the frequency-domain (i.e., after Fourier transformation) are given by

$$\nu_0^{CS} : \frac{\nu_1}{\nu_2} = -p', \tag{22}$$

and

$$\nu_0^{Q} : \frac{\nu_1}{\nu_2} = \frac{C_0(S,p')}{C_0(S,-1)}, \tag{23}$$

where ν_1 and ν_2 are the frequencies along the direct and indirect dimensions.

By applying two shear transformations [6,40,47–51], it is possible to obtain a 2D spectrum corresponding to evolution under only ν_0^{Q} in the indirect dimension (ν_1) and ν_0^{CS} in the direct dimension (ν_2). This can be performed as a similarity transformation, whereby the time variables of the time-domain signal are modified as [47,48,50]

$$s'(\mathbf{t}') = s(\mathscr{A}\mathbf{t}), \tag{24}$$

corresponding to a modification of the frequency-domain data as follows

$$s'(\nu') = s(\mathscr{A}^{-1}\nu) \tag{25}$$

where $\mathbf{t} = \begin{bmatrix} t_1 \\ t_2 \end{bmatrix}$, $\mathbf{t}' = \begin{bmatrix} t_1' \\ t_2' \end{bmatrix}$, $\nu = \begin{bmatrix} \nu_1 \\ \nu_2 \end{bmatrix}$ and $\nu' = \begin{bmatrix} \nu_1' \\ \nu_2' \end{bmatrix}$. The transformation matrix ($\mathscr{A}$) and its inverse ($\mathscr{A}^{-1}$) are given by

$$\mathscr{A} = \begin{bmatrix} -\frac{C_0(S,p')}{C_0(S,p'')} & -1 \\ \frac{p'}{p''} & 1 \end{bmatrix} \tag{26}$$

and

$$\mathscr{A}^{-1} = \begin{bmatrix} \frac{p''C_0(S,p'')}{p'C_0(S,p'')-p''C_0(S,p')} & \frac{p''C_0(S,p'')}{p'C_0(S,p'')-p''C_0(S,p')} \\ -\frac{p''C_0(S,p'')}{p'C_0(S,p'')-p''C_0(S,p')} & -\frac{p''C_0(S,p'')}{p'C_0(S,p'')-p''C_0(S,p')} \end{bmatrix}. \tag{27}$$

In particular, the composite frequency-domain transformation of Eq. (27) can be decomposed into four steps

$$\mathscr{A}^{-1} = \begin{bmatrix} 1 & 0 \\ \phi_1 & 1 \end{bmatrix}\begin{bmatrix} \xi_1 & 0 \\ 0 & 1 \end{bmatrix}\begin{bmatrix} 1 & \phi_2 \\ 0 & 1 \end{bmatrix}\begin{bmatrix} 1 & 0 \\ 0 & \xi_2 \end{bmatrix} = \begin{bmatrix} \xi_1 & \xi_1\xi_2\phi_2 \\ \xi_1\phi_1 & \xi_1\xi_2\phi_1\phi_2 + \xi_2 \end{bmatrix}, \tag{28}$$

which successively describe (from left to right) shearing along ν_1, scaling of the ν_1 axis, shearing along ν_2 and lastly scaling of the ν_2 axis, using the following parameters

$$\phi_1 = -\frac{p'}{p''}, \tag{29}$$

$$\xi_1 = \frac{p''C_0(S,p'')}{p'C_0(S,p'') - p''C_0(S,p')}, \tag{30}$$

$$\phi_2 = 1, \tag{31}$$

$$\xi_2 = 1. \tag{32}$$

The ϕ_1 and ξ_1 terms for all half-integer quadrupolar spins and multiple-quantum transitions are given in Table 1.

Therefore, if the time variables t_1 and t_2 are redefined using Eq. (26),

$$\begin{bmatrix} t_1' \\ t_2' \end{bmatrix} = \mathscr{A}\mathbf{t} = \begin{bmatrix} -\frac{C_0(S,p')}{C_0(S,p'')} & -1 \\ \frac{p'}{p''} & 1 \end{bmatrix}\begin{bmatrix} t_1 \\ t_2 \end{bmatrix} \tag{33}$$

the terms in square brackets of Eq. (20) become

$$C_0(S,p')t_1 + C_0(S,p'')t_2 = -C_0(S,p'')t_1' \tag{34}$$

$$p't_1 + p''t_2 = p''t_2' \tag{35}$$

and the resulting modified time-domain signal is

Table 1
Factors used for shearing and scaling of MQDOR spectra.

S	p	$C_0(S,p)$	ϕ_1	ξ_1
3/2	−1	−3	–	–
	3	−9	3	−1/6
5/2	−1	−8	–	–
	3	6	3	−4/9
	5	−50	5	−4/37
7/2	−1	−15	–	–
	3	27	3	−5/6
	5	−15	5	−1/4
	7	−147	7	−5/64
9/2	−1	−24	–	–
	3	54	3	−4/3
	5	30	5	−4/7
	7	−84	7	−2/13
	9	−324	9	−2/33

$$s'(t_1', t_2') = \exp\{i2\pi\nu_0^{Q}[-C_0(S,p'')]t_1'\}\exp\{-i2\pi\nu_0^{CS}[p'']t_2'\} \tag{36}$$

where evolution of the ν_0^{Q} and ν_0^{CS} terms are isolated into t_1' and t_2', respectively.

3. Experimental details

The sample of $RbNO_3$ was purchased from Strem Chemicals, Inc. and used without further purification. The sample of vitreous B_2O_3 was prepared by melting B_2O_3 powder in a 90Pt/10Rh crucible at 1000 °C for 20 min followed by quenching of the base of the crucible in water. The resulting glass was removed from the crucible and powdered in a nitrogen glove-box prior to loading into the DOR rotor.

All NMR spectra were acquired on a Bruker AVANCE II+ spectrometer at an applied magnetic field of $B_0 = 14.1$ T ($\nu_L(^1H) = 600.1$ MHz) operating at frequencies of 196.3, 57.9 and 192.5 MHz for ^{87}Rb, ^{85}Rb and ^{11}B, respectively. An amplitude-modulated three-pulse z-filtered (Fig. 1) pulse sequence [38,52] was used to record all MQDOR spectra, which yielded 5–10% the sensitivity compared to 1D DOR spectra. The pulse widths (p1, p2 and p3), rf nutation frequencies (ν_{p1}, ν_{p2}, ν_{p3}), spectral widths in the indirect (SW_1) and direct (SW_2) dimensions, number of t_1 increments, number of transients co-added for each t_1 increment, recycle delays, outer rotor (OR) spinning frequencies and total experimental times used for the acquisition of MQDOR spectra are summarized in Table 2. The inner rotor (IR) spinning frequencies were generally in the range of 4.4–4.7 times the OR frequency. Sign discrimination in the indirect dimension was achieved using the States hyper-complex processing method [53]. The desired coherence transfer pathways are selected using a 24-step phase cycle (six steps to select $\Delta p = \pm 3$ on p2, four steps to select $\Delta p = -1$ on p3). In addition, the DOR spectra were acquired with odd-order spinning sideband suppression, which was achieved by synchronization of the excitation and read-out pulses to the outer rotor spin-

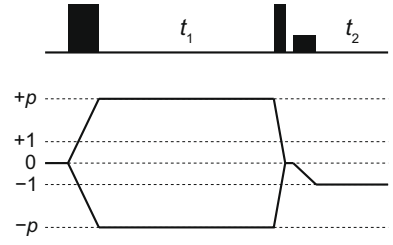

Fig. 1. Three-pulse z-filtered multiple-quantum pulse sequence employed herein for acquisition of MQDOR spectra.

Table 2
Parameters used for acquisition of MQDOR spectra.

Parameter	^{87}Rb	^{85}Rb	^{11}B
p1 [μs]	11.5	15.5	14.5
p2 [μs]	3.75	4.50	4.00
p3 [μs]	10.7	8.25	20.0
ν_{p1} [kHz]	39.0	19.0	37.1
ν_{p2} [kHz]	39.0	19.0	37.1
ν_{p3} [kHz]	11.7	10.1	6.25
SW_1 [kHz]	10.0	20.0	6.39
SW_2 [kHz]	15.0	15.0	28.8
t_1 increments[a]	735	430	92
Transients co-added	192	384	288
Recycle delay [s]	0.15	0.20	1.0
ν_{OR} [Hz]	1400	1306	1600
Experimental time [hours]	21.8	24.5	15.4

[a] Two FIDs were acquired for each t_1 increment for use in 2D hyper-complex processing.

ning frequency as described in Refs. [34,38,54]. Specifically, for the two-dimensional MQDOR experiment, excitation and read-out pulses are synchronized to the IR positions subtending the smallest (up, *u*) and largest (down, *d*) angles with respect to the static magnetic field. Therefore, all pulse and receiver phase steps are kept fixed for four acquisitions as the combination of excitation and read-out pulse synchronization conditions (i.e., *uu*, *ud*, *du*, *dd*) are cycled through. This results in a minimum of 96 steps to complete the phase cycling and the odd-order spinning sideband suppression in both dimensions (see Fig. 1 in Ref. [38]). The $^{85/87}$Rb chemical shifts were referenced to a 0.1 M RbCl aqueous solution with δ_{iso} = 0.0 ppm, while ^{11}B chemical shifts were referenced to neat liquid $(C_2H_5)_2O{\cdot}BF_3$ at 0.0 ppm by using powdered $NaBH_4$ as a secondary reference with $\delta_{iso} = -42.06$ ppm.

4. Crystalline $RbNO_3$ – ^{87}Rb and ^{85}Rb

The crystal structure of $RbNO_3$ has three distinct crystallographic Rb sites [55,56], and has been studied in detail by solid-state NMR [57,58]. A ^{87}Rb triple-quantum DOR (3QDOR) spectrum of $RbNO_3$ is shown in Fig. 2a. The three distinct crystallographic sites of $RbNO_3$ are clearly resolved in ν_2, however, the combination of δ_{CS} and δ_{QS} ($\delta_1 \cdot \nu_L/10^6 = 3\nu_0^{CS} - 9\nu_0^Q$) for sites 2 and 3 cause them to overlap in ν_1. Upon shearing and scaling of ν_1, all three sites become resolved in ν_1 *and* ν_2. The δ_{QS} for each site can readily be measured in ν_1 (Fig. 2b) and P_Q calculated using Eqs. (2), (5), (13), and (18),

$$P_Q[\mathrm{MHz}] = \nu_L\sqrt{\frac{10[2S(2S-1)]^2}{3[3/4 - S(S+1)]}\delta_{QS}} \times 10^{-9}, \tag{37}$$

which yields

$$P_Q[\mathrm{MHz}] = \nu_L\sqrt{-40\delta_{QS}} \times 10^{-9} \quad \text{for } S = 3/2 \tag{38}$$

and

$$P_Q[\mathrm{MHz}] = \nu_L\sqrt{-\frac{500}{3}\delta_{QS}} \times 10^{-9} \quad \text{for } S = 5/2. \tag{39}$$

The P_Q values obtained for the ^{87}Rb sites of $RbNO_3$ are summarized in Table 3. It is particularly noteworthy that the measurement of δ_{QS} values is completely independent of the chemical shift interaction. Determination of P_Q via DOR has often necessitated the acquisition of spectra at multiple magnetic fields, since the lack of characteristic second-order quadrupolar broadening precludes lineshape simulations. The position of signals in DOR spectra will vary at different applied magnetic fields owing to the inverse dependence of δ_{QS} on ν_L (see Eqs. (5) and (18)). Using the MQDOR experiment, an accurate measure of the quadrupolar interaction (P_Q) can be obtained at a single external magnetic field. Subsequent shearing of ν_2 yields δ_{CS} values directly for all three sites (Fig. 2c). The precise temperature of the sample during spectral acquisition (using spinning gases at room temperature) was not determined, this (and the different reference used) is presumably the explanation of the small discrepancy in the δ_{CS} values as compared to those measured in Ref. [58]. The ^{87}Rb P_Q values measured for $RbNO_3$ are in good agreement with results of variable-temperature MQMAS experiments [58] (Table 3), however, much higher accuracy is expected using the method presented herein due to the very small linewidths observed (*vide infra*).

The ^{85}Rb 3QDOR spectrum of $RbNO_3$ is shown in Fig. 3a, where the three distinct sites of $RbNO_3$ can again be clearly distinguished. In this case, the combination of δ_{CS} and δ_{QS} ($\delta_1 \cdot \nu_L/10^6 = 3\nu_0^{CS} + 6\nu_0^Q$)

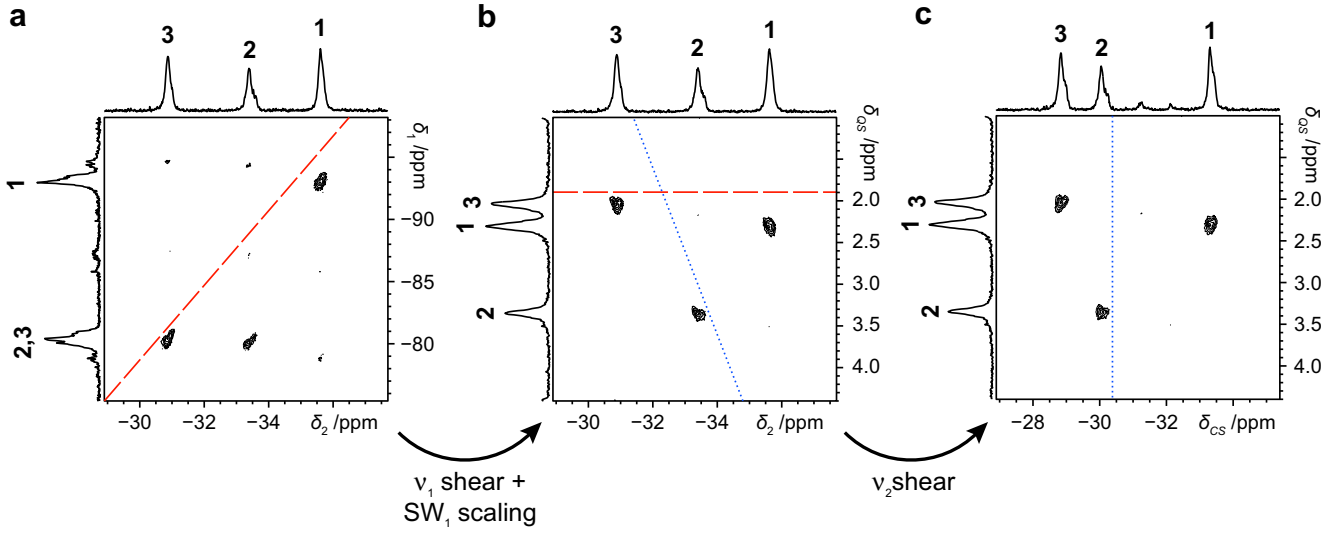

Fig. 2. ^{87}Rb (196.3 MHz) 3QDOR spectra of $RbNO_3$ (a) before and (b) after shearing and scaling of the ν_1 dimension. (c) ^{87}Rb 3QDOR spectrum of $RbNO_3$ after shearing and scaling of ν_1 and ν_2. The gradients of ν_0^{CS} (dashed lines) and ν_0^Q (dotted lines), as well as the numbering of peaks, serve as aids for visualizing the effects of each shear transformation. The base contours are set at 17% of the maximum intensity.

Table 3
^{87}Rb and ^{85}Rb isotropic chemical shift and quadrupolar parameters for the three sites of $RbNO_3$.

Site	δ_{CS}[ppm]	δ_{QS}[ppm]	$\lvert P_Q \rvert$ [MHz]	δ_{CS}[ppm]	$\lvert P_Q \rvert$ [MHz]
	This work			Ref. [58]	
^{87}Rb					
1	−33.4 ± 0.1	−2.31 ± 0.02	1.89 ± 0.01	−32.0[a]	1.88[a]
2	−30.1 ± 0.1	−3.35 ± 0.02	2.27 ± 0.01	−28.4[a]	2.27[a]
3	−28.9 ± 0.1	−2.04 ± 0.02	1.77 ± 0.01	−27.4[a]	1.77[a]
^{85}Rb					
1	−33.4 ± 0.1	−27.2 ± 0.1	3.90 ± 0.01	−32.0[a]	3.89[b]
2	−30.1 ± 0.1	−39.4 ± 0.1	4.70 ± 0.01	−28.4[a]	4.69[b]
3	−28.9 ± 0.1	−24.0 ± 0.1	3.66 ± 0.01	−27.4[a]	3.66[b]

[a] Values obtained for $T \approx 25$ °C using the equations for the δ_{CS} and C_Q obtained from fitting variable-temperature measurements in Ref. [58].
[b] Calculated from the values interpolated for ^{87}Rb using the ratio between the quadrupole moments of ^{85}Rb and ^{87}Rb (Eq. (40)).

causes an overlap of sites 1 and 2 in ν_1. The difference in peak positions for the spectra in Figs. 2a and 3a are caused by the difference in spin quantum numbers and quadrupole moments of ^{85}Rb and ^{87}Rb; note the difference in the ordering of peaks 1–3. By shearing of the ν_1 and ν_2 dimensions (Figs. 3b and 3c) and scaling the ν_1 spectral width, the ^{85}Rb δ_{CS} and δ_{QS} for each site can be measured (Table 3).

The existence of two rubidium isotopes (^{85}Rb and ^{87}Rb) presents an ideal circumstance where the measurement of both chemical shift and quadrupolar parameters can be compared/confirmed at different internal fields for the same chemical system. The isotropic chemical shifts in units of ppm are independent of the isotope observed; this is verified from measurements of δ_{CS} in Figs. 2c and 3c (see Table 3). In contrast, δ_{QS} depends on the spin quantum number, gyromagnetic ratio (γ) and quadrupole moment (Q) of each isotope. The ratio between the quadrupole moments of ^{85}Rb and ^{87}Rb has recently been determined to high accuracy from molecular beam measurements of ^{85}Rb^{19}F and ^{87}Rb^{19}F [59]:

$$\frac{Q(^{87}\mathrm{Rb})}{Q(^{85}\mathrm{Rb})} = 0.4838301 \pm 0.0000018 \qquad (40)$$

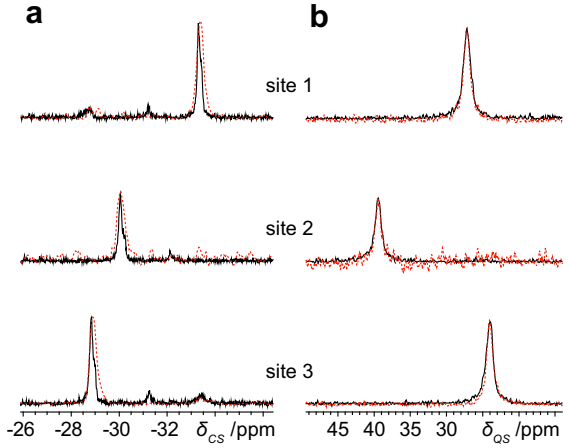

Fig. 4. Projections of the ^{87}Rb and ^{85}Rb MQDOR spectra for the three sites of $RbNO_3$ along the (a) δ_{CS} and (b) δ_{QS} axes after shearing of the ν_1 and ν_2 dimensions. ^{87}Rb and ^{85}Rb spectra are shown as black lines and red dashed lines, respectively. The δ_{QS} axis of ^{87}Rb spectra in (b) have been scaled by the factor in Eq. (41) to facilitate a direct comparison with ^{85}Rb spectra. (For interpretation of the references to color in this figure legend, the reader is referred to the web version of this paper.)

The theoretical ratio between the δ_{QS} of ^{85}Rb and ^{87}Rb can be calculated using Eqs. (2), (5), (18), and (40),

$$\frac{\delta_{QS}(^{85}\mathrm{Rb})}{\delta_{QS}(^{87}\mathrm{Rb})} = \frac{6}{25}\left[\frac{\gamma(^{87}\mathrm{Rb})}{\gamma(^{85}\mathrm{Rb})}\cdot\frac{Q(^{85}\mathrm{Rb})}{Q(^{87}\mathrm{Rb})}\right]^2 \approx 11.775 \qquad (41)$$

Comparison of the δ_{QS} (^{85}Rb) and δ_{QS} (^{87}Rb) values in Table 3 reveals perfect accordance with the expected ratio of Eq. (41) and attests to the validity and accuracy of the approach presented herein.

Projections taken along the δ_{CS} and δ_{QS} dimensions of the ^{85}Rb and ^{87}Rb MQDOR spectra, for the three sites of $RbNO_3$, are shown in Fig. 4. Notably, the δ_{QS}(^{87}Rb) projections in Fig. 4b have been scaled by the factor in Eq. (41) to provide a direct comparison between the spectra of both Rb isotopes. Visual inspection demonstrates excellent correspondence between the ^{85}Rb and ^{87}Rb spectra of $RbNO_3$. Measurement of the full-width at half-height ($\Delta_{1/2}$) for both sets of projections are given in Table 4, where $\Delta^{CS}_{1/2}$

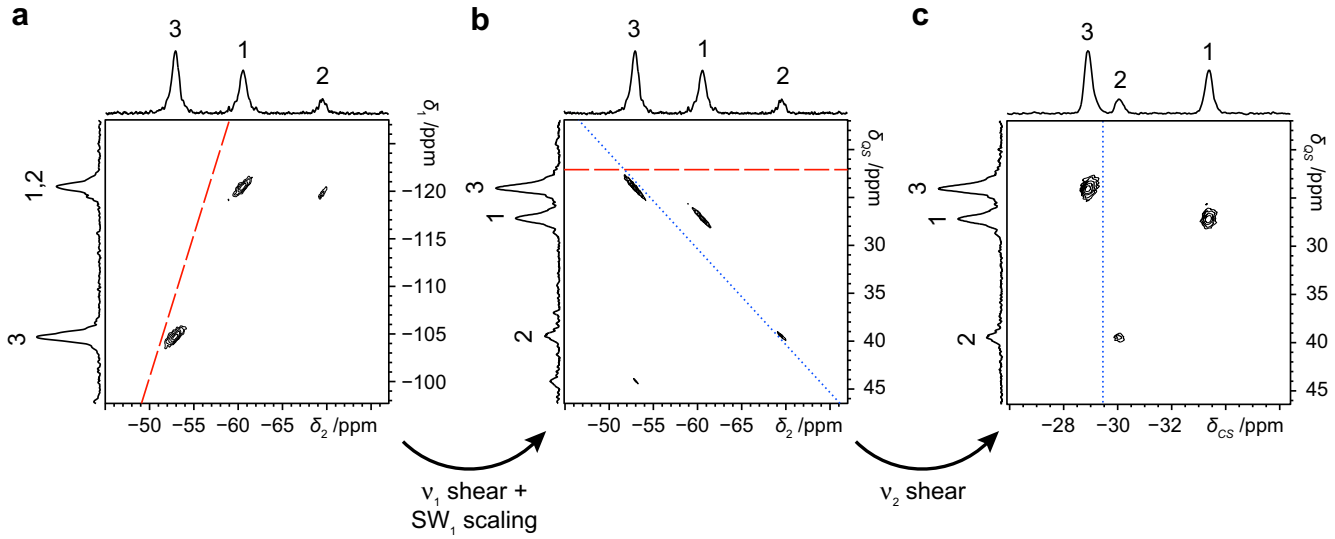

Fig. 3. 2D ^{85}Rb (57.9 MHz) 3QDOR spectra of $RbNO_3$ (a) before and (b) after shearing and scaling of the ν_1 dimension. (c) ^{85}Rb 3QDOR spectrum of $RbNO_3$ after shearing of ν_1 and ν_2. The gradients of ν_0^{CS} (dashed lines) and ν_0^{Q} (dotted lines), as well as the numbering of peaks, serve as aids for visualizing the effects of each shear transformation. The base contours are set at 15% of the maximum intensity.

Table 4
Full-width at half-height ($\Delta_{1/2}$) of δ_{CS} and δ_{QS} projections from ^{87}Rb and ^{85}Rb MQDOR spectra of $RbNO_3$.

Site	$\Delta^{CS}_{1/2}$ [Hz]	[ppm]	$\Delta^{QS}_{1/2}$ [Hz]	[ppm]	$\Delta^{QS}_{1/2}$ [ppm][a]
^{87}Rb					^{85}Rb
1	39.4 ± 0.2	0.201	20.3 ± 0.1	0.103	0.087
2	49.7 ± 0.2	0.253	17.3 ± 0.1	0.088	0.092
3	45.8 ± 0.2	0.233	18.7 ± 0.1	0.095	0.087
^{85}Rb					
1	18.8 ± 0.2	0.324	59.4 ± 0.2	1.03	—
2	21.8 ± 0.2	0.376	63.0 ± 0.2	1.09	—
3	19.0 ± 0.2	0.328	59.4 ± 0.2	1.03	—

[a] $\Delta^{QS}_{1/2}$ (^{87}Rb) values obtained by scaling the $\Delta^{QS}_{1/2}$ (^{85}Rb) by the factor in Eq. (41).

and $\Delta^{QS}_{1/2}$ range from 0.2 to 0.4 and ca. 0.1–1.0 ppm, respectively. Notably the ^{87}Rb $\Delta^{QS}_{1/2}$ values (17.3–20.3 Hz) approach the spin-echo linewidth (i.e., corresponding to the case of the refocusing/removal of inhomogeneous broadening) of 10 Hz determined for $RbNO_3$ by Wang et al. [60]. Detailed inspection of the δ_{CS} (^{87}Rb) projections, with linewidths ~0.2 ppm, reveals fine structure in the peaks of all three sites which might be caused by imperfect shimming. This structure is not observed for ^{85}Rb as the δ_{CS} linewidth in ppm is ~0.35 ppm (~20 Hz) and is probably limited by the intrinsic spin echo T_2. Such linewidths are very small for solid-state NMR of quadrupolar nuclei in systems with a non-zero EFG; the smallest linewidth we have found in the literature is 30 Hz for a 3QMAS spectrum of scandium sulfate [61]. These linewidths are also smaller than the F_2 linewidths in the unshared MQDOR spectra, which correspond to normal 1D DOR spectra (56–75 and 84–96 Hz, respectively, for ^{87}Rb and ^{85}Rb).

5. Vitreous B_2O_3–^{11}B

The small linewidths measured for crystalline $RbNO_3$ serve as a reference to demonstrate that the broader lineshapes in non-crystalline samples arise from distributions in chemical shift and EFG. These types of distributions are hard to obtain using other NMR methods owing to the presence of second-order quadrupolar broadening, which in this instance is averaged by DOR. As an example, the 2D ^{11}B MQDOR spectrum of v-B_2O_3 is shown in Fig. 5 where the presence of two boron sites centered at 14 (non-ring, B_{NR}) and 18 (ring, B_R) ppm is clearly evident. Using the approach described above, after shearing and scaling of ν_1 and ν_2, the projections along ν_1 and ν_2 give isotropic chemical shift and EFG distributions which are completely independent of each other. Close examination of the centerband (Fig. 5, expansion) along ν_1 reveals an approximately linear correlation between δ_{CS} and P_Q for the B_{NR} site, which is much less noticeable for the B_R line. The structure of v-B_2O_3 is of considerable current interest, see Ferlat et al. and references therein [62], detailed analysis of the interaction distributions of v-B_2O_3 using MQDOR NMR is beyond the scope of this article and will be presented elsewhere [63].

6. Conclusions

Acquisition and shearing of two-dimensional triple-quantum MQDOR spectra allows the complete and straightforward separation of the isotropic chemical and quadrupolar shifts which remain under application of DOR. For 3QDOR of $RbNO_3$, linewidths as small as 20 Hz have been measured — we believe these to be the smallest solid-state NMR linewidths measured to date for a half-integer quadrupolar nucleus with a non-zero EFG.

In analogy to the case of MQMAS experiments, higher resolution could be expected for higher-order multiple-quantum coherences depending on the ratio of the homogeneous to inhomogeneous contributions to the isotropic linewidth [61]. It is to be noted, however, that higher-order MQDOR experiments are expected to suffer from reduced sensitivity associated with the excitation and reconversion of the higher-order multiple-quantum coherence as is the case for MQMAS experiments [64,65].

The method presented herein is analogous and complementary to the recently reported COASTER method [40]. By suitable shearing and scaling of triple-quantum, single-quantum two-dimensional correlation spectra recorded at a spinning angle of 70.12°, COASTER separates the chemical shift and quadrupolar *anisotropies* for resolved resonances. In comparison MQDOR removes all anisotropic broadening. As such, the MQDOR experiment is a powerful probe of distributions of isotropic shifts and electric field gradients. It should be particularly useful for investigation of disordered systems where these distributions give different information about the material. This is demonstrated here for vitreous B_2O_3, for which the separate distributions of and correlation between isotropic chemical shift and EFG are experimentally determined.

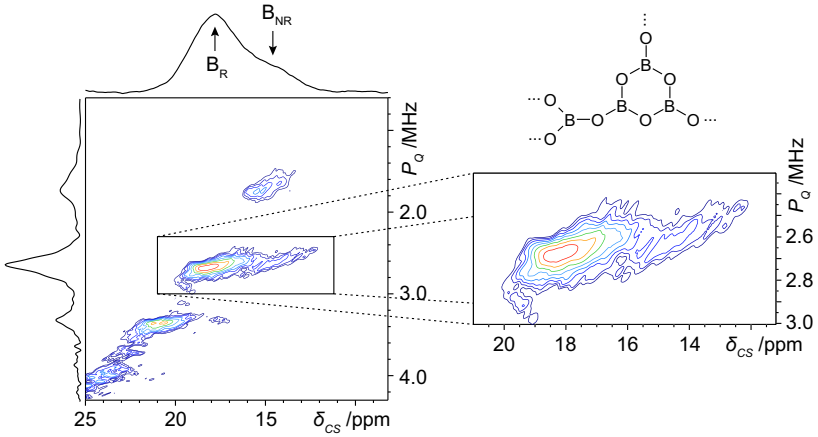

Fig. 5. ^{11}B (192.5 MHz) 3QDOR spectrum of v-B_2O_3 after shearing and scaling of ν_1 and ν_2. Arrows denote the center of gravity for the distinct ring (B_R) and non-ring (B_{NR}) boron sites. The inset shows an expansion of the centerband along the ν_1 dimension; note the linear correlation between δ_{CS} and P_Q (calculated from δ_{QS} using Eq. (38)) for the B_{NR} site. The base contours are set at 14% of the maximum intensity.

Acknowledgments

Funding from EPSRC, BBSRC and the University of Warwick is acknowledged. I.H. and R.D. thank the Leverhulme Trust for funding. A.W. thanks the NSERC of Canada for a Post-Doctoral Fellowship Award.

References

[1] A. Llor, J. Virlet, Towards high-resolution NMR of more nuclei in Solids—sample spinning with time-dependent spinner axis angle, Chem. Phys. Lett. 152 (1988) 248–253.
[2] A. Samoson, E. Lippmaa, A. Pines, High-resolution solid-state NMR averaging of secon-order effects by means of a double-rotor, Mol. Phys. 65 (1988) 1013–1018.
[3] K.T. Mueller, B.Q. Sun, G.C. Chingas, J.W. Zwanziger, T. Terao, A. Pines, Dynamic-angle spinning of quadrupolar nuclei, J. Magn. Reson. 86 (1990) 470–487.
[4] L. Frydman, J.S. Harwood, Isotropic spectra of half-integer quadrupolar spins from bidimensional magic-angle-spinning NMR, J. Am. Chem. Soc. 117 (1995) 5367–5368.
[5] A. Medek, J.S. Harwood, L. Frydman, Multiple-quantum magic-angle spinning NMR: a new method for the study of quadrupolar nuclei in solids, J. Am. Chem. Soc. 117 (1995) 12779–12787.
[6] S.P. Brown, S. Wimperis, Two-dimensional multiple-quantum MAS NMR of quadrupolar nuclei: a comparison of methods, J. Magn. Reson. 128 (1997) 42–61.
[7] Z.H. Gan, Isotropic NMR spectra of half-integer quadrupolar nuclei using satellite transitions and magic-angle spinning, J. Am. Chem. Soc. 122 (2000) 3242–3243.
[8] S.E. Ashbrook, S. Wimperis, High-resolution NMR of quadrupolar nuclei in solids: the satellite-transition magic angle spinning (STMAS) experiment, Prog. Nucl. Magn. Reson. Spectrosc. 45 (2004) 53–108.
[9] B.F. Chmelka, K.T. Mueller, A. Pines, J. Stebbins, Y. Wu, J.W. Zwanziger, O-17 NMR in solids by dynamic-angle spinning and double rotation, Nature 339 (1989) 42–43.
[10] K.T. Mueller, Y. Wu, B.F. Chmelka, J. Stebbins, A. Pines, High-resolution O-17 NMR of solid silicates, J. Am. Chem. Soc. 113 (1991) 32–38.
[11] Z. Xu, B.L. Sherriff, Al-27 double-rotation NMR-study of Al_2 Sio_5 polymorph minerals, Appl. Magn. Reson. 4 (1993) 203–211.
[12] D. Massiot, D. Muller, T. Hubert, M. Schneider, A.P.M. Kentgens, B. Cote, J.P. Coutures, W. Gessner, Double-rotation and magic-angle-spinning nuclear-magnetic-resonance study of Al-27—Re-examination of the aluminium borate $9Al_2O_3.2B_2O_3$, Solid State Nucl. Magn. Reson. 5 (1995) 175–180.
[13] R.E. Youngman, S.T. Haubrich, J.W. Zwanziger, M.T. Janicke, B.F. Chmelka, Short-range and intermediate-range structural ordering in glassy boron-oxide, Science 269 (1995) 1416–1420.
[14] K.J.D. MacKenzie, M.E. Smith, M. Schmucker, H. Schneider, P. Angerer, Z. Gan, T. Anupold, A. Reinhold, A. Samoson, Structural aspects of mullite-type $NaAl_9$ O_{14} studied by Al-27 and Na-23 solid-state MAS and DOR NMR techniques, Phys. Chem. Chem. Phys. 3 (2001) 2137–2142.
[15] D. Prochnow, A.R. Grimmer, D. Freude, Solid-state NMR studies of O-17-enriched pyrophosphates, Solid State Nucl. Magn. Reson. 30 (2006) 69–74.
[16] I. Hung, A.P. Howes, T. Anupold, A. Samoson, D. Massiot, M.E. Smith, S.P. Brown, R. Dupree, Al-27 double rotation two-dimensional spin diffusion NMR: complete unambiguous assignment of aluminium sites in $9Al_2$ O_3.2B2 O3, Chem. Phys. Lett. 432 (2006) 152–156.
[17] C. Rohrig, I. Dierdorf, H. Gies, X-ray-powder diffraction and NMR-spectroscopic investigations on a porous zincosilicate related to the zeolite VPI-7, J. Phys. Chem. Solids 56 (1995) 1369–1376.
[18] R. Jelinek, A. Malek, G.A. Ozin, Na-23 synchronized double-rotation NMR-study of Cs^+, $Ca2^+$, and $La3^+$ cation-exchanged sodium zeolite-Y, J. Phys. Chem. 99 (1995) 9236–9240.
[19] L.M. Bull, B. Bussemer, T. Anupold, A. Reinhold, A. Samoson, J. Sauer, A.K. Cheetham, R. Dupree, A high-resolution O-17 and Si-29 NMR study of zeolite siliceous ferrierite and ab initio calculations of NMR parameters, J. Am. Chem. Soc. 122 (2000) 4948–4958.
[20] J.E. Readman, C.P. Grey, M. Ziliox, L.M. Bull, A. Samoson, Comparison of the O-17 NMR spectra of zeolites LTA and LSX, Solid State Nucl. Magn. Reson. 26 (2004) 153–159.
[21] A. Stein, G.A. Ozin, G.D. Stucky, Class-B sodalites—nonstoichiometric silver, sodium halosodalites, J. Am. Chem. Soc. 114 (1992) 8119–8129.
[22] G. Engelhardt, P. Sieger, J. Felsche, Multinuclear solid-state NMR of host-guest systems with TO2 (T = Si, Al) host-frameworks—a case-study on sodalites, Anal. Chim. Acta 283 (1993) 967–985.
[23] G. Engelhardt, H. Koller, P. Sieger, W. Depmeier, A. Samoson, Aluminum-27 and sodium-23 double-rotation NMR of sodalites, Solid State Nucl. Magn. Reson. 1 (1992) 127–135.
[24] M.P.J. Peeters, J.W. Dehaan, L.J.M. Vandeven, J.H.C. Vanhooff, Hydration Of $AlPO_4$-11 studied with X-ray-powder diffraction and Al-27 and P-31 NMR, J. Phys. Chem. 97 (1993) 5363–5369.
[25] J. Janchen, M.P.J. Peeters, J.W. Dehaan, L.J.M. Vandeven, J.H.C. Vanhooff, I. Girnus, U. Lohse, Adsorption calorimetric measurements and Al-27 DOR NMR-studies on the molecular-sieve $AlPO_4$-18, J. Phys. Chem. 97 (1993) 12042–12046.
[26] Y. Wu, D. Lewis, J.S. Frye, A.R. Palmer, R.A. Wind, Cross-polarization double-rotation NMR, J. Magn. Reson. 100 (1992) 425–430.
[27] Y. Wu, B.F. Chmelka, A. Pines, M.E. Davis, P.J. Grobet, P.A. Jacobs, High-Resolution Al-27 NMR-spectroscopy of the aluminophosphate molecular-sieve VPI-5, Nature 346 (1990) 550–552.
[28] A. Samoson, P. Sarv, J.P.V. Houckgeest, B. Kraushaarczarnetzki, Chemical-Shift Anisotropy of Al-27 in $AlPO_4$-21, Appl. Magn. Reson. 4 (1993) 171–178.
[29] V. Lemaitre, K.J. Pike, A. Watts, T. Anupold, A. Samoson, M.E. Smith, R. Dupree, New insights into the bonding arrangements of L- and D-glutamates from solid state O-17 NMR, Chem. Phys. Lett. 371 (2003) 91–97.
[30] K.J. Pike, V. Lemaitre, A. Kukol, T. Anupold, A. Samoson, A.P. Howes, A. Watts, M.E. Smith, R. Dupree, Solid-state O-17 NMR of amino acids, J. Phys. Chem. B 108 (2004) 9256–9263.
[31] A. Wong, K.J. Pike, R. Jenkins, G.J. Clarkson, T. Anupold, A.P. Howes, D.H.G. Crout, A. Samoson, R. Dupree, M.E. Smith, Experimental and theoretical O-17 NMR study of the influence of hydrogen-bonding on C=O and O—H oxygens in carboxylic solids, J. Phys. Chem. A 110 (2006) 1824–1835.
[32] A. Wong, A.P. Howes, K.J. Pike, V. Lemaitre, A. Watts, T. Anupold, J. Past, A. Samoson, R. Dupree, M.E. Smith, New limits for solid-state O-17 NMR spectroscopy: complete resolution of multiple oxygen sites in a simple biomolecule, J. Am. Chem. Soc. 128 (2006) 7744–7745.
[33] A.P. Howes, T. Anupold, V. Lemaitre, A. Kukol, A. Watts, A. Samoson, M.E. Smith, R. Dupree, Enhancing resolution and sensitivity of ^{17}O solid-state NMR through combining double rotation, ^1H decoupling and satellite modulation for biomolecular applications, Chem. Phys. Lett. 421 (2006) 42–46.
[34] I. Hung, A. Wong, A.P. Howes, T. Anupold, J. Past, A. Samoson, X. Mo, G. Wu, M.E. Smith, S.P. Brown, R. Dupree, Determination of NMR interaction parameters from double rotation NMR, J. Magn. Reson. 188 (2007) 246–259.
[35] A. Wong, I. Hung, A.P. Howes, T. Anupold, J. Past, A. Samoson, S.P. Brown, M.E. Smith, R. Dupree, The determination of O-17 NMR parameters of hydroxyl oxygen: a combined deuteration and DOR approach, Magn. Reson. Chem. 45 (2007) S68–S72.
[36] A. Samoson, Two-dimensional isotropic NMR of quadrupole nuclei in solids, J. Magn. Reson. Ser. A 121 (1996) 209–211.
[37] T. Anupold, A. Reinhold, P. Sarv, A. Samoson, A comparison of double rotation and multi-quantum magic angle spinning spectra, Solid State Nucl. Magn. Reson. 13 (1998) 87–91.
[38] A. Samoson, T. Anupold, Synchronized double rotation 2D NMR, Solid State Nucl. Magn. Reson. 15 (2000) 217–225.
[39] A.P.M. Kentgens, E.R.H. van Eck, T.G. Ajithkumar, T. Anupold, J. Past, A. Reinhold, A. Samoson, New opportunities for double rotation NMR of half-integer quadrupolar nuclei, J. Magn. Reson. 178 (2006) 212–219.
[40] J.T. Ash, N.M. Trease, P.J. Grandinetti, Separating chemical shift and quadrupolar anisotropies via multiple-quantum NMR spectroscopy, J. Am. Chem. Soc. 130 (2008) 10858–10859.
[41] B.Q. Sun, J.H. Baltisberger, Y. Wu, A. Samoson, A. Pines, Sidebands in dynamic angle spinning (DAS) and double rotation (DOR) NMR, Solid State Nucl. Magn. Reson. 1 (1992) 267–295.
[42] E. Cochon, J.P. Amoureux, Side-band analysis in DOR NMR-Spectra.1. Infinite inner-rotor speed, Solid State Nucl. Magn. Reson. 2 (1993) 205–222.
[43] J.P. Amoureux, E. Cochon, Side-band analysis in DOR NMR-Spectra.2. Real finite inner-rotor speed, Solid State Nucl. Magn. Reson. 2 (1993) 223–234.
[44] J. Skibsted, N.C. Nielsen, H. Bildsoe, H.J. Jakobsen, V-51 MAS NMR-spectroscopy—determination of quadrupole and anisotropic shielding tensors, including the relative orientation of their principal-axis systems, Chem. Phys. Lett. 188 (1992) 405–412.
[45] A.P.M. Kentgens, A practical guide to solid-state NMR of half-integer quadrupolar nuclei with some applications to disordered systems, Geoderma 80 (1997) 271–306.
[46] R.N. Zare, Angular Momentum: Understanding Spatial Aspects in Chemistry and Physics, John Wiley and Sons, New York, 1988.
[47] K. Nagayama, P. Bachmann, K. Wuthrich, R.R. Ernst, Use of cross-sections and of projections in 2-dimensional NMR-spectroscopy, J. Magn. Reson. 31 (1978) 133–148.
[48] K. Nagayama, A. Kumar, K. Wuthrich, R.R. Ernst, Experimental-techniques of two-dimensional correlated spectroscopy, J. Magn. Reson. 40 (1980) 321–334.
[49] P.J. Grandinetti, J.H. Baltisberger, A. Llor, Y.K. Lee, U. Werner, M.A. Eastman, A. Pines, Pure-absorption-mode lineshapes and sensitivity in 2-dimensional dynamic-angle spinning NMR, J. Magn. Reson. Ser. A 103 (1993) 72–81.
[50] P.J. Grandinetti, Y.K. Lee, J.H. Baltisberger, B.Q. Sun, A. Pines, Side-band patterns in dynamic-angle-spinning NMR, J. Magn. Reson. Ser. A 102 (1993) 195–204.
[51] D. Massiot, B. Touzo, D. Trumeau, J.P. Coutures, J. Virlet, P. Florian, P.J. Grandinetti, Two-dimensional magic-angle spinning isotropic reconstruction sequences for quadrupolar nuclei, Solid State Nucl. Magn. Reson. 6 (1996) 73–83.
[52] J.P. Amoureux, C. Fernandez, S. Steuernagel, Z filtering in MQMAS NMR, J. Magn. Reson. Ser. A 123 (1996) 116–118.
[53] D.J. States, R.A. Haberkorn, D.J. Ruben, A two-dimensional Nuclear Overhauser experiment with pure absorption phase in 4 quadrants, J. Magn. Reson. 48 (1982) 286–292.
[54] A. Samoson, E. Lippmaa, Synchronized double-rotation NMR spectroscopy, J. Magn. Reson. 84 (1989) 410–416.

[55] M. Shamsuzzoha, B.W. Lucas, Structure (Neutron) of phase-IV rubidium nitrate at 298 and 403 K, Acta Crystallogr. Sect. B-Struct. Commun. 38 (1982) 2353–2357.
[56] C. Dean, T.W. Hambley, M.R. Snow, Structures of phase-IV rubidium nitrate, $RbNO_3$, and phase-II cesium nitrate, $CsNO_3$, Acta Crystallogr. Sect. C-Cryst. Struct. Commun. 40 (1984) 1512–1515.
[57] J.H. Baltisberger, S.L. Gann, E.W. Wooten, T.H. Chang, K.T. Mueller, A. Pines, Rb-87 dynamic-angle spinning NMR-spectroscopy of inorganic rubidium salts, J. Am. Chem. Soc. 114 (1992) 7489–7493.
[58] J. Skibsted, H.J. Jakobsen, Variable-temperature Rb-87 magic-angle spinning NMR spectroscopy of inorganic rubidium salts, J. Phys. Chem. A 103 (1999) 7958–7971.
[59] J. Cederberg, E. Frodermann, H. Tollerud, K. Huber, M. Bongard, J. Randolph, D. Nitz, Nuclear electric quadrupole moments of Rb from the hyperfine spectrum of RbF, J. Chem. Phys. 124 (2006) 244304.
[60] S.H. Wang, Z. Xu, J.H. Baltisberger, L.M. Bull, J.F. Stebbins, A. Pines, Multiple-quantum magic-angle spinning and dynamic-angle spinning NMR spectroscopy of quadrupolar nuclei, Solid State Nucl. Magn. Reson. 8 (1997) 1–16.
[61] K.J. Pike, R.P. Malde, S.E. Ashbrook, J. McManus, S. Wimperis, Multiple-quantum MAS NMR of quadrupolar nuclei. Do five-, seven- and nine-quantum experiments yield higher resolution than the three-quantum experiment?, Solid State Nucl Magn. Reson. 16 (2000) 203–215.
[62] G. Ferlat, T. Charpentier, A.P. Seitsonen, A. Takada, M. Lazzeri, L. Cormier, G. Calas, F. Mauri, Boroxol rings in liquid and vitreous B_2O_3 from first principles, Phys. Rev. Lett. 101 (2008) 065504.
[63] I. Hung, A.P. Howes, B. Parkinson, T. Anupõld, A. Samoson, S.P. Brown, D. Holland, P.F. Harrison, R. Dupree, Determination of the bond-angle distribution in vitreous $B_2\ O_3$ by ^{11} B double rotation (DOR) NMR spectroscopy, (submitted for publication)..
[64] J.P. Amoureux, C. Fernandez, L. Frydman, Optimized multiple-quantum magic-angle spinning NMR experiments on half-integer quadrupoles, Chem. Phys. Lett. 259 (1996) 347–355.
[65] J.P. Amoureux, C. Fernandez, Triple, quintuple and higher order multiple-quantum MAS NMR of quadrupolar nuclei, Solid State Nucl. Magn. Reson. 10 (1998) 211–223.